MAGNETOHYDRODYNAMICS Vol. 51 (2015), No. 2, pp. 215–224

EXPERIMENTAL AND THEORETICAL STUDY OF THE DYNAMICS OF WAKES GENERATED BY MAGNETIC OBSTACLES

D.R. Domínguez[1], *A. Beltrán*[2], *J.J. Román*[1], *S. Cuevas*[1], *E. Ramos*[1]

[1] *Renewable Energy Institute, Universidad Nacional Autónoma de México 62580, Temixco Mor. Mexico*

[2] *Materials Research Institute (Morelia Unit), Universidad Nacional Autónoma de México, 58190, Morelia, Mich., Mexico*

We present an experimental and theoretical study of the dynamics of wakes generated by magnetic obstacles. The experimental obstacle was realized by circulating a liquid metal inside a closed loop with a slender cross-section and imposing a fixed localized magnetic field in a specific spot of the loop. Experimental observations made with an Ultrasonic Doppler Velocimeter include records of the axial velocity of liquid metal as a function of the axial coordinate in the region where the wake of the obstacle is formed. This information reveals important features of the stability and dynamics of the wake of the magnetic obstacle. The theoretical study is based on a numerical solution of a quasi-two dimensional model of the MHD balance equations whose non-dimensional form indicates that the flow can be described in terms of two parameters, the Reynolds and the Hartmann numbers. The numerical model considers the induced magnetic field as an electromagnetic variable (B-formulation). Theoretical studies predict that for a given Hartmann number, the flow transits from a steady state to a time-dependent state as the Reynolds number is increased as in the wake of a rigid obstacle, but in sharp contrast to this case, when the Reynolds number is increased further, the flow becomes steady again. Our experimental observations confirm that this prediction is correct.

Introduction. The term magnetic obstacle is used to denote the Lorentz force that opposes the flow of an electrically conducting fluid due to the presence of a localized magnetic field. The relative motion between the fluid and the applied magnetic field induces electric currents that interact with the field and generate a localized Lorentz force that acts as an obstacle for the flow. In the 1970's, it was realized that complex velocity structures could appear in flows under non-uniform magnetic fields [1], although experimental results were not able to confirm this fact [2]. In the last decade, several studies (mainly theoretical) have explored the flow past magnetic obstacles and described important physical features [3]–[12]. The first studies used a numerical approach to provide a quasi-two-dimensional description of the flow in conditions, where inertial effects were not negligible [3], and under creeping flow conditions [4]. It was shown that both time-dependent and steady vortical flows that in some aspects resemble flows past bluff bodies, may appear. Through numerical simulation and experiments, other studies revealed that a steady six-vortex pattern that was not observed in hydrodynamic flows could appear in the wake of a magnetic obstacle at certain values of the Reynolds number Re, interaction parameter N (or equivalently the Hartmann number Ha) and constrainment factor κ defined as the ratio of the lateral size of the magnet exposed to the oncoming flow to the width of the channel [5, 6]. The analogy between flows past solid and magnetic obstacles has been investigated, recognizing that important differences exist between these two physical situations [7, 8]. Other numerical simulation studies have shown that the imposition of magnetic fields of different strengths may give rise to transitional flow regimes for a fixed Reynolds and different values of the interaction parameter, observing vortex shedding phe-

nomena as well as sustained turbulent bursts close to the magnetic wake region [9]. Recently, the influence of a localized non-uniform magnetic field on liquid metal flow was investigated numerically using the quasi-static approximation to analyze the three-dimensional flow transformation and the generation of vortex structures by a strong magnetic dipole field [10]. An important feature of the wakes generated by magnetic obstacles, detected with the ultrasonic velocity profile method, is that the length of the recirculation region behind the magnetic obstacle increases with the Reynolds number to reach a maximum and then decreases [11]. Preliminary theoretical studies indicate that for large enough Hartmann numbers, increasing the Reynolds number results in the formation of a wake behind the magnetic obstacle with similar features to a von Kármán vortex street that occurs behind a rigid obstacle, but in sharp contrast to the dynamic behavior of the wake formed by a rigid obstacle; a further increase of the Reynolds number leads to a reduction of vortex shedding behind the magnetic obstacle [12]. In the present contribution, we extend the study presented in [12] by describing the experimental recordings that were made to detect the axial velocity of the flow of liquid metal in the presence of a magnetic obstacle with the objective of determining representative properties of the wake. The observations show that for a fixed Hartmann number, the energy contained in the vortices of the wake does present a maximum as a function of the Reynolds number, indicating that the obstacle sheds vorticity to the ambient in a finite range of Reynolds numbers.

1. Experimental setup. The experimental device used in the observations described in this paper is a rectangular loop made from acrylic (Polymethyl methacrylate) walls with a rectangular effective cross-section of 1 cm × 8 cm. The lengths of the large and short legs of the duct are 85.8 cm and 40 cm, respectively. The loop is built in sections joined with flanges and the whole system is fixed with mounts that separate it from the floor of the table, making it easier to detect possible leaks. An MHD induction pump with rotating permanent magnets is located straddling one of the long legs. The pump consists of a motor that spins two disks where 24 permanent neodymium magnets are mounted radially; this device sets the liquid metal in motion around the loop. The velocity of the liquid metal is measured by a Signal Processing ultrasonic Doppler velocimeter (UDV) using a probe of 0.8 cm in diameter and a wave frequency of 4 MHz. With this equipment, it is possible to determine one component of the velocity along the propagation line of the acoustic wave emerging from the emitter. The ultrasonic gauge was fixed at the downstream end of the region of analysis to detect the axial velocity along the axial coordinate. An appropriate mount was used to place the gauge at different vertical positions. The flow generated by the pump is characterized using the Reynolds number defined as $\mathrm{Re} = U D_\mathrm{h}/\nu$, where U is the average axial velocity, D_h is the hydraulic diameter of the cross-section and ν is the kinematic viscosity of the working fluid (see below). Given that the geometry of the duct and the physical properties of the fluid are fixed, the range of Reynolds numbers available with the experimental equipment depends on the power delivered by the pump (or equivalently the pressure difference) and on the resistance of the duct. We determined the range of the Reynolds number available through direct measurement of the axial velocity. Our measurements indicated that $869 < \mathrm{Re} < 4960$.

A photograph of the experimental device indicating the position of the MHD pump, the magnets and the UDV system, is shown in Fig. 1. The design of our equipment follows closely that of similar facilities developed at the Technical University of Ilmenau, Germany (see, for instance, [14] and [15]). A sketch showing the position of the magnets and the UDV, together with some details of the flow,

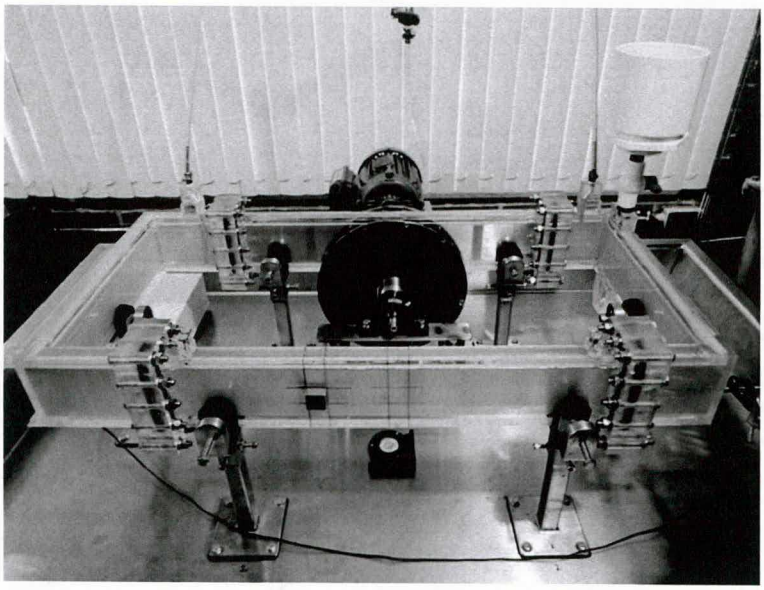

Fig. 1. The experimental liquid metal loop. The MHD pump is in the far long leg. The disks with permanent magnets and the liquid metal rotate in the counterclockwise direction. The magnet that generates the magnetic obstacle is close to the central part of the near long leg, 30 cm away from the upstream corner and 4 cm above the lower wall of the duct. The ultrasonic gauge is in the far right of the picture near the duct corner.

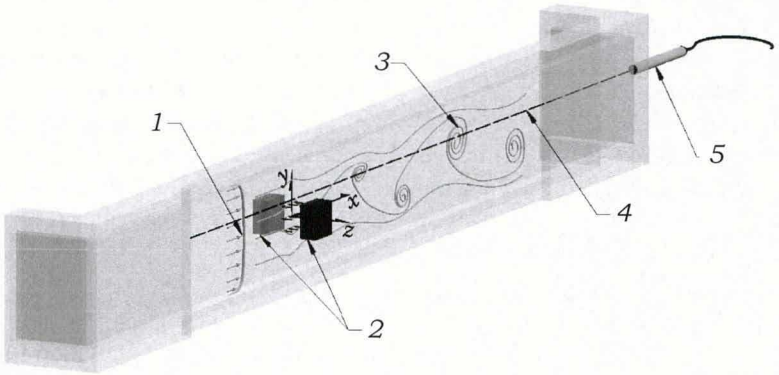

Fig. 2. Sketch of the observation zone and position of the axis of coordinates. *1* – upstream velocity profile, *2* – magnets, *3* – wake of the magnetic obstacle, *4* – line for ultrasonic Doppler velocity recordings, *5* – ultrasonic Doppler velocimetry probe.

and the axes of coordinates used in the numerical study are shown in Fig. 2.

The working fluid is a Ga(68%)In(20%)Sn(12%) eutectic mixture which has a melting temperature of 10.5°C and a kinematic viscosity of $\nu = 3.3 \times 10^{-7}$ m^2/s. The magnetic obstacle is created by two 2.54 cm × 2.54 cm× 1.25 cm neodymium magnets placed on the outer side of the opposite vertical walls of the central part of one of the long legs. The magnets are located 30 cm away from the upstream corner and 4 cm from the lower horizontal wall of the duct. With this magnet arrangement, the maximum magnetic field that can be obtained at the center of the duct is 0.23 T, and the constrainment factor is $\kappa = 0.31$ (side of the magnet/height of the duct). A second non dimensional parameter that characterizes the flow is

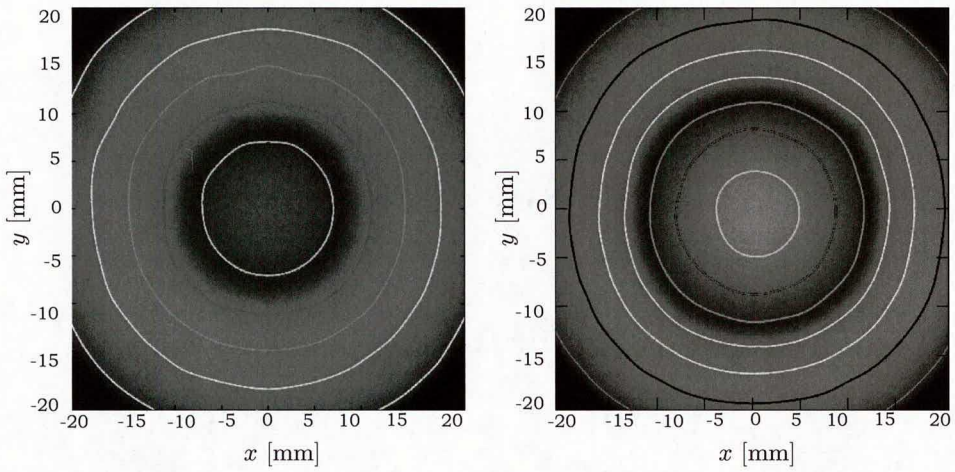

Fig. 3. Magnetic field distribution at the center of the duct for Hartmann numbers 58 (left) and 75 (right). The central circles represent 0.125 T and 0.175 T for Hartmann numbers 58 and 75, respectively. In the two cases, the contours are separated 0.025 T.

the Hartmann number defined as $\mathrm{Ha} = B_0 D\sqrt{\sigma/\rho\nu}$, where B_0 is the maximum strength of the magnetic field at the center of the duct, D is the gap between the vertical walls of the duct, and σ and ρ are the electric conductivity and the density of the working fluid, respectively. For GaInSn, $\sigma = 3.46\times10^6\ 1/\Omega\mathrm{m}$ and $\rho = 6360\,\mathrm{kg/m^3}$. The range of Hartmann numbers available depends on the intensity of the permanent magnets used and their relative position with respect to the liquid metal, but increasing the distance of the magnets to the vertical walls reduces the effective magnitude of the magnetic field inside the duct and also reduces the Hartmann number. In Fig. 3, we show the distribution of the normal component of the magnetic field for distances of 3.6 cm and 3.1 cm between the magnets. These conditions yield Hartmann numbers of 58 and 75, respectively. As can be appreciated, both magnetic fields have similar to Gaussian distributions, but with different spread and maximum values. As it is usual in liquid metal MHD duct flows, the magnetic Reynolds number defined as $\mathrm{Rm} = \mu_0\sigma U D$ is very small.

2. Numerical model. A quasi two-dimensional (Q2D) model is proposed to simulate the MHD flow through a spatially localized magnetic field produced by magnets fixed to the channel walls. This simplified model can be regarded as a first approach that captures the dominant physical effects without going into the complexities of a full three dimensional model. Within this approximation, only the component of the magnetic field normal to the vertical walls is considered. The origin of the axis of coordinates is located on the line that joins the geometrical center of the magnets and the halfway between the vertical walls of the duct (see Fig. 2). The dimensionless axial (x) and vertical (y) coordinates increase in the downstream and upward directions, respectively, and are scaled with the side length of the magnet L. The traversal coordinate (z) is defined in the direction perpendicular to the vertical walls and scaled by D. The main assumption of the Q2D model is that the transport of momentum in the z-direction is mainly diffusive so that the velocity components can be expressed in the form

$$u(x,y,z,t) = \tilde{u}(x,y,t)f(x,y,z), \quad v(x,y,z,t) = \tilde{v}(x,y,t)f(x,y,z), \qquad (1)$$

where $\tilde{u}$ and $\tilde{v}$ are the z-averaged velocity components in the x- and y-directions, respectively. The velocity components are scaled by the average axial velocity U.

The function f considers the variation of the velocity profile in the z-direction and must satisfy the normalization condition $\int_{-1/2}^{1/2} f\,\mathrm{d}z = 1$. Its dependence on the x and y coordinates must reflect the different flow regions due to the localization of the magnetic field. Details of the quasi-two dimensional model can be found in [3]. The friction function f can be obtained from the following balance between the viscous and the Lorentz force

$$\frac{\mathrm{d}^2 f}{\mathrm{d}z^2} - \left(\mathrm{Ha}\, B_z^0(x,y)\right)^2 f = \varepsilon^2 \mathrm{Re}\frac{\mathrm{d}p}{\mathrm{d}x}, \tag{2}$$

where ε is the aspect ratio D/L. The terms on the left-hand side correspond to the viscous and induced Lorentz forces, while the term on the right-hand side is an externally imposed axial pressure gradient which generates the duct flow and is constant. It should be noted that due to the normalization for f, this parameter does not appear explicitly in the solution. The function f must satisfy no-slip conditions at both vertical walls $f(z = \pm 1/2) = 0$. The solution that satisfies the boundary and normalization conditions has the form

$$f = -\mathcal{H}a\, \mathrm{e}^{-\mathcal{H}a(z+0.5)} \times \frac{\mathrm{e}^{\mathcal{H}a} - \mathrm{e}^{2\mathcal{H}a} - \mathrm{e}^{\mathcal{H}a(z+0.5)} + \mathrm{e}^{\mathcal{H}a(z+2.5)} + \mathrm{e}^{\mathcal{H}a(1+2z)} - \mathrm{e}^{2\mathcal{H}a(1+z)}}{4\mathrm{e}^{\mathcal{H}a} + (1 - \mathrm{e}^{2\mathcal{H}a})(\mathcal{H}a + 2)}, \tag{3}$$

where $\mathcal{H}a = \mathrm{Ha}B_z^0$ is defined as the local Hartmann number.

In order to obtain the z-average from the conservation equations, we substitute expressions (1) and (3) into the governing MHD equations and integrate in the z-direction. Dropping the tilde, the dimensionless averaged equations of motion take the form

$$\frac{\partial u}{\partial x} + \frac{\partial v}{\partial y} = 0, \tag{4}$$

$$\frac{\partial u}{\partial t} + u\frac{\partial u}{\partial x} + v\frac{\partial u}{\partial y} = -\frac{\partial p}{\partial x} + \frac{1}{\mathrm{Re}}\nabla_\perp^2 u + \frac{u}{\tau} + \frac{\mathrm{Ha}^2}{\varepsilon^2 \mathrm{Re}} j_y B_z^0, \tag{5}$$

$$\frac{\partial v}{\partial t} + u\frac{\partial v}{\partial x} + v\frac{\partial v}{\partial y} = -\frac{\partial p}{\partial y} + \frac{1}{\mathrm{Re}}\nabla_\perp^2 v + \frac{v}{\tau} - \frac{\mathrm{Ha}^2}{\varepsilon^2 \mathrm{Re}} j_x B_z^0, \tag{6}$$

where the pressure p, the electric current density components j_x and j_y, and the applied field $B_z^0(x,y)$ are scaled by ρU^2, $\sigma U B_0$, and B_0, respectively. The sub index $\perp$ denotes the projection of the nabla operator on the (x,y)-plane. The time t is normalized by L/U. The model shows that there are two nondimensional parameters, the Reynolds (Re) and the Hartmann (Ha) number (for definitions see Section 1). The third term on the right-hand side of Eqs. (5) and (6) represents the Hartmann–Rayleigh friction and arises due to the boundary layers at the Hartmann walls. The Hartmann–Rayleigh friction can be conveniently represented in terms of a characteristic dimensionless timescale τ, which indicates the decay of vorticity due to dissipation in the Hartmann and viscous layers. The inverse of this time scale is given by

$$\tau^{-1} = \frac{1}{\varepsilon^2\ \mathrm{Re}}\left.\frac{\mathrm{d}f}{\mathrm{d}z}\right|_{-1/2}^{1/2} = -\frac{1}{\varepsilon^2 \mathrm{Re}}\frac{2\mathcal{H}a^2(\mathrm{e}^{\mathcal{H}a}+1)^2}{4\mathrm{e}^{\mathcal{H}a} + (1-\mathrm{e}^{2\mathcal{H}a})(\mathcal{H}a+2)}. \tag{7}$$

In the quasi-static approximation the magnetic induction equation takes the form

$$\nabla_\perp^2 b_z - u\frac{\partial B_z^0}{\partial x} - v\frac{\partial B_z^0}{\partial y} = 0, \tag{8}$$

where the induced magnetic field b_z has been normalized by $\mathrm{Rm}B_0$. Once b_z is determined, Ampere's law gives an expression to calculate electric currents, namely,

$$j_x = \frac{\partial b_z}{\partial y} \qquad \text{and} \qquad j_y = -\frac{\partial b_z}{\partial x}. \tag{9}$$

A solution to the quasi two-dimensional model model given in Eqs. (4)–(9) is sought via numerical methods. The finite volume method described in [16] on an orthogonal equi-distant grid was used to solve the conservation equations (4)–(8). The distribution of the applied magnetic field $B_z^0(x, y)$ required for the numerical solution is a fit of the experimental magnetic field (Fig. 3) with the expression given by [13] for a square surface magnetized in the normal direction. The numerical solution was obtained in a rectangular domain of 35×3.2 non-dimensional units using a grid of 700×256. The boundary conditions consider no-slip conditions for the velocity components at $y = \pm 1.6$. At the inlet ($x = -10$), a uniform velocity profile is used, whereas Neumann boundary conditions are imposed at the outlet ($x = 25$). We assume that the induced magnetic field is zero $b_z = 0$ at all boundaries. The standard time-marching procedure (Euler method) was used for the time integration with a non-dimensional time step of 5×10^{-4}.

3. Results. Exploratory observations indicate that the flow generated by the magnetic obstacle is a very complex, three dimensional, time dependent phenomenon, whose comprehensive description would require a large research program. In the present study, we concentrate on a very specific aspect of this flow, namely, in the detection of vortical structures in the wake as functions of the Reynolds number. Before we present quantitative results, it is convenient to describe some qualitative features of the flow. The axial velocity u in the (x, t) space for the vertical position $y = 12.7\,\mathrm{mm}$ is plotted in Fig. 4. The left panel displays the experimental recordings obtained with UDV for Ha = 75 and Re = 2300, and the right panel shows similar results obtained with the numerical solution using Ha = 80 and Re = 2500. A zoom is provided for the experimental results. An interesting feature of the experimental records is that the axial velocity just upstream the magnetic obstacle is reduced (red-purple vertical strip at $-50\,\mathrm{mm} < x < 0\,\mathrm{mm}$) and then it increases in the region $0\,\mathrm{mm} < x < 140\,\mathrm{mm}$. The inclined, red and

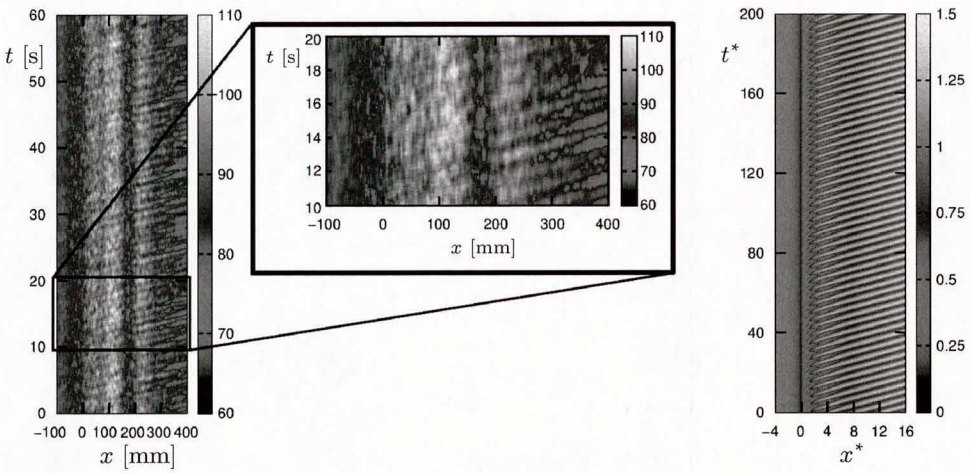

Fig. 4. Map of the axial velocity u in the (x,t) space, $y = 12.7\,\mathrm{mm}$. Left: UDV experimental observations for Ha = 75, Re = 2300. Right: numerical calculation for Ha = 80, Re = 2500.

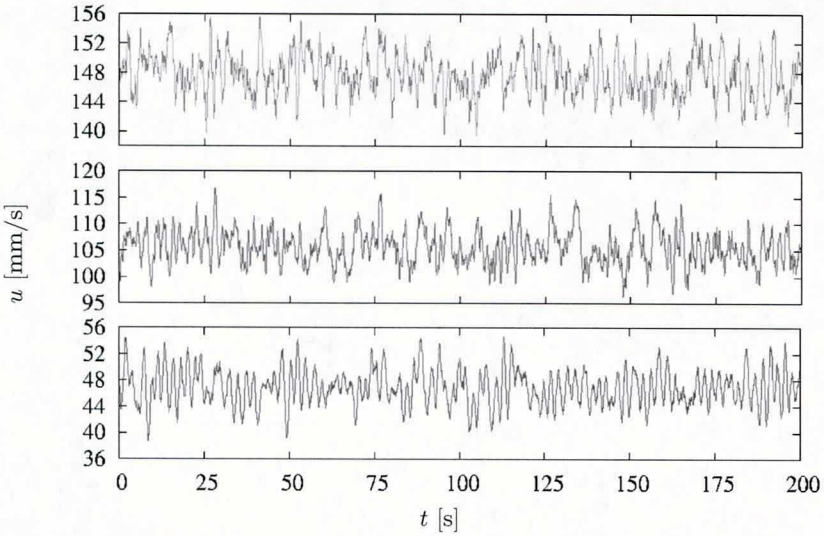

Fig. 5. Experimental axial velocity u as a function of time at the point $x = 400\,\text{mm}$, $y = 12.7\,\text{mm}$ for Ha = 75. Starting from the top, traces were obtained for Re = 1272, 3163 and 4568. Note the different scales in the ordinates of the three graphs and that the largest amplitude corresponds to Re = 3163.

purple parallel strips in the region $x > 170\,\text{mm}$ indicate the transit of a periodic perturbation in time for a fixed point in space, or in space for a snapshot. This velocity pattern is consistent with vortex shedding with an approximate characteristic time of the order of 1.0 s. The results obtained with the numerical solution display similar features, with periodic inclined parallel strips that indicate the transit of periodic structures.

In order to a make a more specific analysis, we show in Fig. 5 a sample of the axial velocity traces observed at a fixed point ($x = 400\,\text{mm}$, $y = 12.7\,\text{mm}$) as a function of time for Ha = 75 and Re = 1272, 3163 and 4568. The sampling frequency was 20 Hz. The original traces were smoothed with a moving average filter of 15 points, equivalent to a sampling rate of 0.75 s. As seen, the traces are irregular, with many Fourier modes involved, and also the average amplitude of the perturbations is not a monotonous function of the Reynolds number. Note that the time average of the signals increases with the Reynolds number, as expected, but in contrast, we find that the amplitude of the velocity fluctuations is larger for the case Re=3163 than for of the other two cases in Fig. 5. With the velocity traces alone, it is difficult to quantify the amplitude difference between the different cases and, in the following, we will develop methods to obtain a more quantitative assessment. The average velocity obtained by experimental and numerical methods is of the same order of magnitude, indicating that this feature is correctly captured with the model. However, the oscillations superimposed to the average flow calculated numerically have single or few Fourier modes, with periods of approximately 3.7 non-dimensional units. See also the right panel of Fig. 4.

An alternative way of displaying the previous results that is more amenable for comparison is to plot the parameter $\mathcal{A}$ defined by

$$\mathcal{A} = u - \langle u \rangle, \tag{10}$$

where $\langle u \rangle$ is the average axial velocity over a time interval I_0. In Fig. 6, we show 40 s of the readings of the variable $\mathcal{A}$ as a function of time for the same Reynolds numbers analyzed in Fig. 5 and using $I_0 = 53\,\text{s}$ (10^3 readings). Inspection

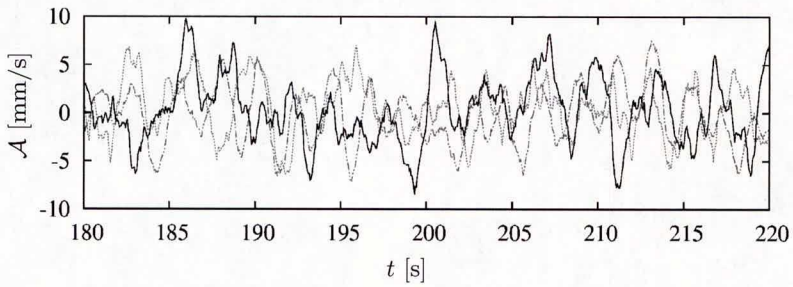

Fig. 6. The parameter $\mathcal{A}$ as a function of time for three Reynolds numbers: Re = 1272 (blue line-dots), 3163 (black continuous line) and 4568 (red dots).

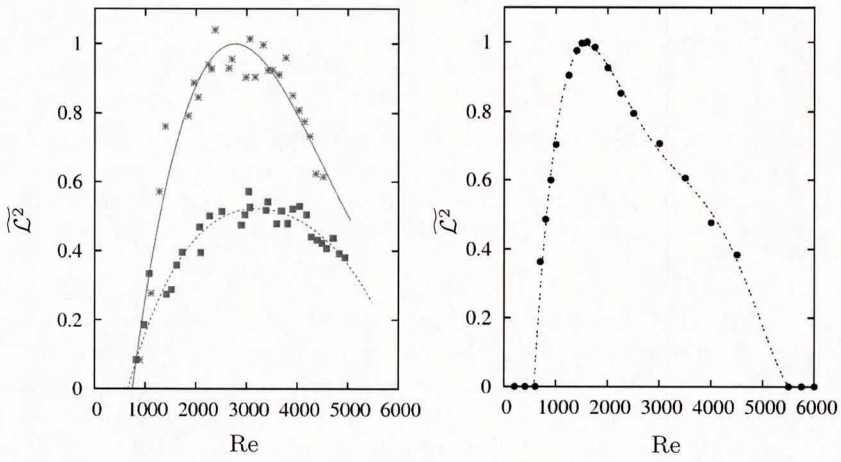

Fig. 7. The parameter $\widetilde{\mathcal{L}^2}$ as a function of the Reynolds number. Left panel: experimental observations. Ha = 58 (blue line with squares) and Ha = 75 (red line with asterisks). The lines are fits to the experimental data. The fits of $\widetilde{\mathcal{L}^2}$ attain maxima at Re = 3190 and 2750 for Ha = 58 and 75, respectively. Right panel: theoretical calculations. Ha = 80, the maximum is attained at approximately Re = 600.

indicates that the amplitude of the traces is of the order of 10 mm/s and that the amplitude of the perturbations obtained with Re = 3163 is larger than that found in the other cases. The corresponding properties of the flow obtained with numerical integration show that the amplitude of the oscillation is much smaller (approximately of 0±25 mm/s), which is by a factor of 20 smaller than the observed experimental value.

In order to make a quantitative comparison, we define the parameter $\mathcal{L}^2$ as

$$\mathcal{L}^2 = \frac{1}{I}\int_0^I \mathcal{A}^2 \mathrm{d}t. \tag{11}$$

Note that $\mathcal{L}^2$ is a function of the Hartmann and Reynolds numbers only and indicates the average of the square of the amplitude of the axial velocity oscillation with respect to its average value in the interval I which is related to the kinetic energy of the vortices in the wake.

In the left panel of Fig. 7 we show the experimental results for $\mathcal{L}^2$ at Ha = 58 and 75 as functions of the Reynolds number. The actual data shown in the figure and denoted by $\widetilde{\mathcal{L}^2}$ are normalized with the maximum (smoothed) value of $\mathcal{L}^2$(Ha = 75). As it can be seen from the figure, the trends of $\widetilde{\mathcal{L}^2}$ are not

monotonous but display maxima. Our experimental device allows us to capture data for very small values, which leads us to determine the critical Reynolds number, where the first bifurcation occurs, i.e. where the wake of the magnetic obstacle becomes time dependent; $\widehat{\mathcal{L}^2}$ is zero for Reynolds numbers smaller than the critical ones. The first critical Reynolds number is found at approximately 900 for the two cases explored. The experimental equipment prevents us to obtain data for Reynolds numbers larger than approximately 5000 for Ha = 58 and 75, but in the two cases, the data display an unmistakeable trend towards smaller values. Extrapolating the experimental data available, the Reynolds number where $\widehat{\mathcal{L}^2}$ reduces to zero, is approximately 6000 for Ha = 75, but for Ha = 58 it is difficult to estimate the Reynolds number, where the energy of the perturbations in the wake vanishes. The maxima of the smoothed data are attained at Re = 3190 and 2750, respectively, for Ha = 58 and 75. The trend displayed by $\widehat{\mathcal{L}^2}$ obtained with the numerical solution and considering Ha = 80 is shown in the right panel of Fig. 7. The data have been normalized with their maximum value. The variable $\widehat{\mathcal{L}^2}$ obtained by numerical calculations displays qualitative features similar to those observed in the experiment, and the range of Reynolds numbers where the wake of the obstacle sheds vortices, is approximately the same for theory and experiment, but the amplitude is not. The latter is a consequence of the fact that the model underestimates the amplitude of the velocity fluctuations, as indicated in the discussion of Fig. 6.

4. Conclusion. Experimental records of the wake formed by a magnetic obstacle in a liquid metal flow made by an ultrasonic velocimeter are presented. The velocity readings show intermittent perturbations that indicate vortex shedding from the magnetic obstacle. We observe that for small Reynolds numbers ($300 < \mathrm{Re} < 700$) the energy of the perturbations in the wake increases to reach a maximum that depends on the Hartmann number. Then the energy reduces monotonically up to the maximum Reynolds number that can be reached with our experimental equipment. This indicates that the oscillatory wake is present in the flow only in a finite range of Reynolds numbers. This observation is in qualitative agreement with a quasi-two-dimensional theory also presented in this report. Although a more detailed study of the behavior near the first critical Reynolds number where the steady flow becomes time dependent is required, the data available indicates that the first bifurcation is a supercritical Hopf bifurcation (for a definition see [17]). The first critical Reynolds number detected is much larger than the rigid cylindrical obstacle (approximately 45 [18]); this effect may be due to the stabilizing effect of the lateral walls. Unfortunately, our experimental equipment prevents us to explore the nature of the inverse bifurcation found at large Reynolds numbers, but the numerical solution suggests that it is an inverse supercritical Hopf bifurcation.

The numerical model used to simulate the specific feature of the flow analyzed in this contribution does capture the magnitude of the average velocity correctly, but fails to give good results on the complexity and magnitude of the velocity fluctuations.

Acknowledgments. We deeply thank the Research Training Group Lorentz Force Velocimetry at the Ilmenau University of Technology, Germany, for helpful discussions and advice for the construction of the experimental set up. D.R. Domínguez and J.J. Román received MSc and PhD grants from CONACYT (Mexico). Financial support from CONACYT (Mexico) through project no. 240785 is gratefully acknowledged.

REFERENCES

[1] Y.M. Gelfgat, D.E. Peterson, and E.V. Shcherbinin. Velocity structure of flows in non-uniform constant magnetic fields 1. Numerical calculations. *Magnetohydrodynamics*, vol. 14 (1978), no. 1, pp. 55–61.

[2] Y.M. Gelfgat, and S.V. Olshanskii. Velocity structure of flows in non-uniform constant magnetic fields. II. Experimental results. *Magnetohydrodynamics*, vol. 14 (1978), no. 2, pp. 151–154.

[3] S. Cuevas, S. Smolentsev, and M.A. Abdou. On the flow past a magnetic obstacle. *J. Fluid Mech.*, vol. 553 (2006), pp. 360–365.

[4] S. Cuevas, S. Smolentsev and M.A. Abdou. Vorticity generation in the creeping flow past a magnetic obstacle. *Phys. Rev. E*, vol. 74 (2006), 056301.

[5] E.V. Votyakov, Y. Kolesnikov, O. Andreev, E. Zienicke, and A. Thess. Structure of the wake of a magnetic obstacle. *Phys. Rev. Lett.*, vol. 98 (2007), 144504.

[6] E.V. Votyakov, E. Zienicke, and Y.B. Kolesnikov. Constrained flow around a magnetic obstacle. *J. Fluid Mech.*, vol. 610 (2008), pp. 131–156.

[7] E.V. Votyakov and S.C. Kassinos. On the analogy between streamlined magnetic and solid obstacles. *Phys. Fluids*, vol. 21 (2009), no. 9, 097102.

[8] E.V. Votyakov and S.C. Kassinos. Core of the magnetic obstacle. *J. Turbulence*, vol. 11 (2010), pp. 1468–5248.

[9] S. Kenjeres, S. ten Cate, C.J. Voesenek. Vortical structures and turbulent burst behind magnetic obstacles in transitional flow regimes. *Int. J. Heat Fluid Flow*, vol. 32 (2011), no. 3, pp. 510–528.

[10] S. Tympel, T. Boeck, and J. Schumacher. Laminar and transitional liquid metal duct flow near a magnetic point dipole. *J. Fluid Mech.*, vol. 735 (2013), pp. 553–586.

[11] O. Andreev, Y. Kolesnikov, and A. Thess. Application of the ultrasonic velocity profile method to the mapping of liquid metal flows under the influence of a non-uniform magnetic field. *Exp. Fluids*, vol. 49 (2009), pp. 77–83.

[12] E. Ramos, A. Beltrán, S. Cuevas and S. Smolentsev. Dynamic properties of a magnetic obstacle. In: *Book of Abstracts of the 7th International* PAMIR *Conference.* Presqu'île de Giens, France, 2008, vol. 2, pp. 891–895.

[13] M. McCaig. Permanent Magnets in Theory and Practice. (Wiley, 1977).

[14] D. Jian and C. Karcher. Electromagnetic flow measurements in liquid metals using time-of-flight Lorentz force velocimetry. *Meas. Sci. Tech.*, vol. 23 (2012), no. 7, p. 074021.

[15] C. Heinicke. Spatially resolved measurements in a liquid metal flow with Lorentz force velocimetry. *Exp. Fluids*, vol. 54 (2013), no. 6, p. 18.

[16] H.K. Versteeg and W. Malalasekera. An Introduction to Computational Fluid Dynamics: The Finite Volume Method. (Longman Scientific and Technical, 1995).

[17] S. Lynch. Dynamical Systems With Applications Using Matlab. (Birkhauser, Boston, 2004).

[18] C.H.K. Williamson. Vortex dynamics in the cylinder wake. *Annual Review of Fluid Mechanics*, vol. 28 (1996), pp. 477–539.

Received 20.12.2014